

# Estimating Imaging Artifacts Caused by Internal Multiples

Alison E. Malcolm\*, Maarten V. de Hoop, Center for Wave Phenomena, Colorado School of Mines  
Henri Calandra, Total

## Summary

Imaging with seismic data is typically carried out under the assumption of single scattering. Here we illustrate a theory that includes multiply scattered waves in the imaging process. We estimate artifacts in the image caused by internal multiples rather than estimating the multiples themselves in the data. The theory behind this approach comes from a series derived from the Lippmann-Schwinger equation and the Bremmer coupling series. From this theory two images are formed, one with all the data and the other with the estimated artifacts from first-order internal multiples. The construction of the second image requires knowledge of the velocity model to the depth of the up to down reflection in the internal multiple. We illustrate this theory with a synthetic data example and examine the sensitivity of the method to the velocity model.

## Introduction

We develop an explicit scheme for modeling and imaging with triply scattered waves, which can be extended to higher order scattering by recursion. This scheme is integrated in the downward continuation, or ‘wave-equation’, approach to migration and estimates the artifacts in the image caused by internal multiples, rather than estimating the multiples themselves. We require knowledge of the velocity model to the depth of the shallowest reflector involved in the triple scattering. This is implicitly the depth where the image is currently being formed.

In our approach, we develop a hybrid series between the Lippmann-Schwinger series [6] and the generalized Bremmer coupling series [3]. Both these series have been used for SRME [1, 10], as well as for internal multiple attenuation [10, 5, 8]. Our approach does not require the traveltime monotonicity condition introduced by ten Kroode [8], and can be used in the presence of caustics.

## The scattering series

We model multiple scattering through a hybrid between the generalized Bremmer and Lippmann-Schwinger series. Let the components of  $U$  denote the up- and down-going wave constituents and the subscript indicate how many times the constituent has scattered, then

$$\begin{aligned} \delta U_1(\hat{V}) &= D_t^2 \mathbf{L}_0(\hat{V}U_0), \\ \text{and } \delta U_m(\hat{V}) &= D_t^2 \mathbf{L}_0(\hat{V}\delta U_{m-1}(\hat{V})). \end{aligned} \quad (1)$$

Here  $\hat{V}$  represents a matrix of reflectivities, and  $\mathbf{L}_0$  denotes the diagonal matrix of one-way propagators (or Green’s functions) evaluated in the background velocity model. Let  $R$  denote the restriction of the wavefield to depth  $z = 0$ , and ( $\mathcal{H}$  denotes the Hilbert transform in time)

$$\mathbf{Q} = \frac{1}{2} \begin{pmatrix} (Q_+^*)^{-1} & -\mathcal{H}Q_+ \\ (Q_-^*)^{-1} & \mathcal{H}Q_- \end{pmatrix} \quad (2)$$

represent the operator that decomposes the wavefield into its up- and down-going constituents. We define  $\mathbf{M}_0 = R\mathbf{Q}^{-1}\mathbf{L}_0$ . The data are then modeled as

$$\delta D = \left( \frac{d}{\partial_z d} \right) = -D_t^2 \mathbf{M}_0(\hat{V}(U_0 + \sum_{m \in \mathbb{N}} (-1)^{m+1} \delta U_m(\hat{V}))). \quad (3)$$

The leading order term on the right-hand side represents the singly scattered or Born contribution. This contribution is written explicitly in terms of the propagator  $H$  of the double-square-root (DSR) equation as

$$\begin{aligned} d_1(s_0, r_0, t) &= \frac{1}{4} D_t^2 Q_{-,r_0}^*(0) Q_{-,s_0}^*(0) \int_0^\infty dz_1 H(0, z) \\ &Q_{-,r_1}(z_1) Q_{-,s_1}(z_1) (E_1 E_2 a)(z_1, s_1, r_1, t_0), \end{aligned} \quad (4)$$

where

$$\begin{aligned} E_1 &: a'(z, x) \mapsto \delta(r-s) a'(z, \frac{r+s}{2}), \\ E_2 &: a(z, r, s) \mapsto \delta(t) a(z, r, s), \end{aligned}$$

while  $a = 2c_0^{-3} \delta c$  if  $c_0$  denotes the smooth background velocity and  $\delta c$  denotes the velocity contrast. In the above, we note that the propagator of the wave equation,  $G$ , is related to the one-way propagators by  $G = Q_-^* G_- Q_-$  for the up-going constituents. Together the  $E_1$  and  $E_2$  operators represent the adjoint of the imaging condition; they take an image and create from it data with  $t = 0$  and  $s = r$ .

## Inverse scattering

In inverse scattering the goal is to solve for  $\hat{V}$  in terms of the data  $d$  (cf. (3)). We write the series

$$\hat{V} = \sum_{m \in \mathbb{N}} \hat{V}_m(d) \quad (5)$$

subject to the following relation between the  $\hat{V}_m = \hat{V}_m(d)$ ,

$$\begin{aligned} -D_t^2 \mathbf{M}_0(\hat{V}_1 U_0) &= \delta D \\ D_t^2 \mathbf{M}_0(\hat{V}_m U_0) &= D_t^4 \mathbf{M}_0(\hat{V}_{m-1} \mathbf{L}_0(\hat{V}_1 U_0)) \quad m > 1. \end{aligned} \quad (6)$$

## Artifacts due to Internal Multiples

From this it follows that

$$-D_t^2 \mathbf{M}_0(\widehat{V}U_0) = \delta D - \left( \sum_{m \in \mathbb{N}} D_t^2 \mathbf{M}_0(\widehat{V}_m \delta U) \right). \quad (7)$$

If we ignore the second term on the right-hand side, the problem of expressing  $\widehat{V}$  in terms of the data reduces to inverse scattering in the Born approximation [7]. The single-scattering imaging procedure can be split into two steps. First, from (4) the downward continuation to depth  $z$ ,

$$\tilde{d}_1(z) = H(0, z)^* Q_{-,s}^*(0)^{-1} Q_{-,r}^*(0)^{-1} d, \quad (8)$$

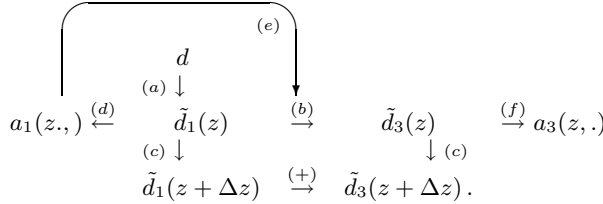
followed by application of the imaging condition

$$a_1(z, \cdot) = R_1 W^{-1} \psi R_2 D_t^{-2} \tilde{d}_1(z) \quad (9)$$

where  $R_1 = E_1^*$  and  $R_2 = E_2^*$  are the usual imaging conditions ( $t = 0$  and  $h = 0$ ), and  $W$  is directly related to  $Q_{-,s}(z)Q_{-,r}(z)$ . The pseudodifferential operator,  $\psi$ , accounts for amplitude corrections [7]. We apply (8)-(9) to (7), from which we obtain an image (first term on the right-hand side) minus artifacts (second term).

### Artifacts due to internal multiples in imaging

The estimation of artifacts in imaging from triply scattered waves is obtained in the following way:

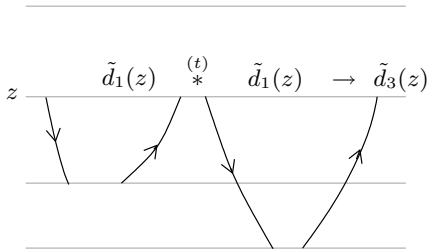


(a) We use (8) to estimate  $\tilde{d}_1(z)$ , the data downward continued to the depth  $z$ .

(b) We estimate  $\tilde{d}_3$ , the triply scattered data downward continued to depth  $z$  given by

$$\tilde{d}_3(z, s, r, t) = D_t^2 \iint Q_{-,s'}^*(z) (E_1 a)(z, s', r') Q_{-,r'}^*(z) \tilde{d}_1(z, s', r, \cdot) \overset{(t)}{*} \tilde{d}_1(z, s, r', \cdot) ds' dr' \quad (10)$$

restricting  $\tilde{d}_1$  to  $t > 0$ ; this equation is illustrated below



Note the similarity between (10) and the SRME procedure [4, 2, 9].

(c) We downward continue to the next depth, making use of the relation

$$d_3(s_0, r_0, t) = Q_{-,r_0}^*(0) Q_{-,s_0}^*(0) H(0, z) \tilde{d}_3(z, \cdot). \quad (11)$$

(d) We apply (9) to  $\tilde{d}_1$  to generate the image.

(e) The image estimated in (d) feeds back into the estimation of the multiples; this appears as the  $(E_1 a)(z, s', r')$  factor in (10).

(f) We estimate the artifacts in the image by applying (9) to  $\tilde{d}_3$ , i.e.,

$$a_3(z, \cdot) = R_1 W^{-1} \psi R_2 D_t^{-2} \tilde{d}_3(z). \quad (12)$$

The estimate of  $a_3$  can then be subtracted from the estimate of  $a_1$  to form the final image estimate.

### Lens Model

We illustrate the method with a synthetic data example. The velocity model is shown in Figure 1 and consists of a single layer beneath a low-velocity lens. The lens is located in the center of the model; it is circular with Gaussian velocity variations, a diameter of 600 m and a maximum contrast of  $-2$  km/s. Shot records were generated at a spacing of 10 m from a lateral distance of 9 to 11 km, using finite difference modeling. We use a double-square-root propagator that works in midpoint-offset coordinates rather than shot and receiver. To accommodate this choice, we use a subset of the available offsets so that each midpoint has the same number of offsets. The data from a midpoint of 9.8 km are shown in Figure 2. The first arrival is highlighted in this figure to show the triplications caused by the lens more clearly.

To estimate the multiple, we propagate the data to 2 km, the top of the layer, and again show the cmp at midpoint 9.8 km in Figure 3 along with the estimated multiples at this depth. Note that the caustic has been removed by the propagation through the lens and that the multiple is accurately estimated. Both the data and the estimated multiples are propagated through the model, forming an image at each depth step. Figure 4 compares the estimated artifact with the artifact seen in the image; AGC has been applied to highlight the artifact in the image.

To illustrate the dependence of this method on the background velocity model, we perturb the velocity and estimate the artifacts caused by internal multiples in the incorrect velocity model. In theory, from equations (11) and (12), knowledge of the velocity is necessary only to the depth of the shallowest reflection, in this case the top of the layer at 2 km depth. To test this we add a second lens, with properties identical to the first lens, below the layer. Because the perturbation depends on midpoint the estimated multiple also depends on midpoint. Although the estimated artifact does not match the image artifact as well in this case as when the correct velocity is used, the estimate remains quite good, as shown in Figure 5.

## Artifacts due to Internal Multiples

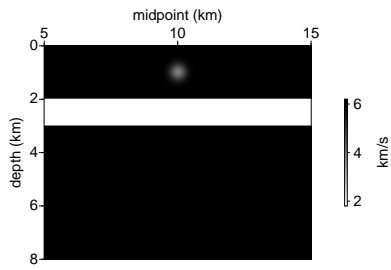


Fig. 1: Velocity model consisting of a single layer beneath a low-velocity lens.

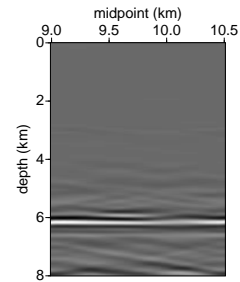
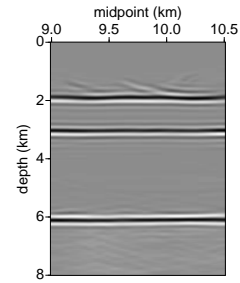


Fig. 4: Top: Image with an artifact from the first-order internal multiple at approximately 6 km depth. Bottom: Estimated artifacts from first-order internal multiples.

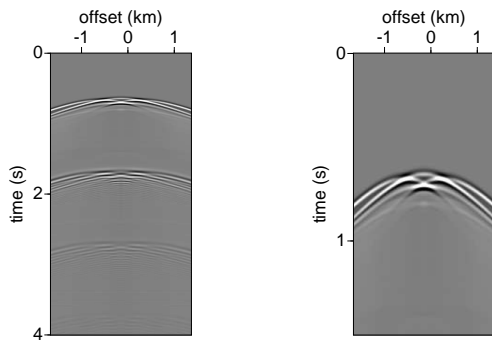


Fig. 2: Common midpoint gather at 9.8 km and zero depth, with only the offsets used to compute the images shown later. Note the triplications caused by the lens. Left: full gather. Right: zoom of the primary reflection from the top layer.

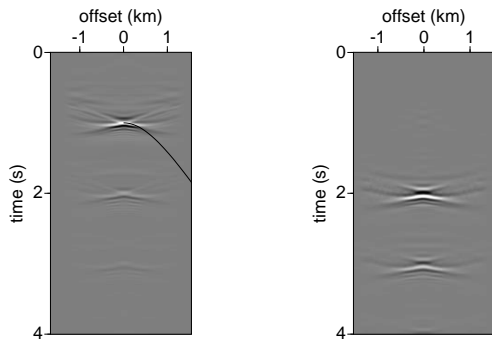


Fig. 3: Left: Common midpoint gather at 9.8 km and 2 km depth, after the  $t \leq 0$  times have been removed. Note the disappearance of the multi-pathing as the data are now below the lens. The solid line shows the expected moveout curve for the reflection from the bottom of the reflector. Right: estimated multiples at this depth.

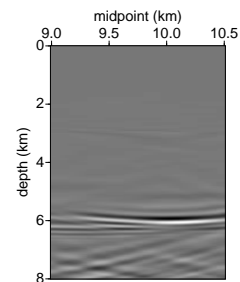
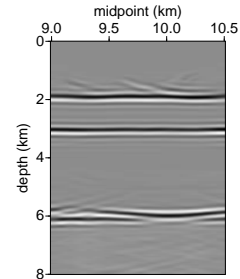


Fig. 5: In these images, a second lens has been added beneath the layer to introduce a laterally varying velocity perturbation. Top: Image with artifacts from internal multiples. Bottom: Estimated artifacts from first-order internal multiples.

## Artifacts due to Internal Multiples

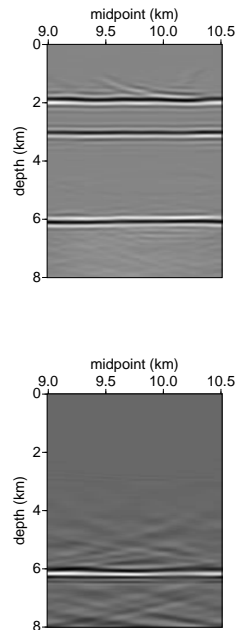


Fig. 6: In this model the lens was moved 0.2 km deeper than in the correct velocity model. Because this perturbation is above the top of the layer, we expect this to have an impact on the estimated multiple. Note the phase difference between the estimated artifact and the image. Top: Image with artifacts from first-order internal multiples. Bottom: Estimated artifacts from first-order internal multiples.

The theory presented here does require knowledge of the velocity model to the depth of the up to down reflection (top of layer at 2 km depth). To test the sensitivity of the method to errors in this velocity, we move the lens 200 m shallower than in the correct velocity model. In Figure 6, we demonstrate that we can still estimate the multiple with reasonable accuracy with this velocity perturbation.

## Discussion

We have described a method to estimate imaging artifacts caused by first-order internal multiples. This method requires knowledge of the velocity model down to the top of the layer that generates the multiple (the depth of the up-to-down reflection). The main computational cost of the algorithm comes from the downward continuation of the data and the internal multiples. By estimating the multiple on downward continued data, rather than in surface data, we avoid difficulties caused by caustics in the wavefield or the failure of the traveltime monotonicity assumption. In addition, estimating artifacts in the image rather than estimating multiples in the data shows clearly which part of the image has been contaminated by internal multiples, even if those multiples are poorly estimated or incompletely subtracted.

## References

- [1] F. Aminzadeh and J. M. Mendel. On the brekker series decomposition: Equivalence between two different approaches. *Geophysical Prospecting*, 28:71–84, 1980.
- [2] A. J. Berkhout and D. J. Verschuur. Estimation of multiple scattering by iterative inversion, part I: Theoretical considerations. *Geophysics*, 62(5):1586–1595, 1997.
- [3] M. V. de Hoop. Generalization of the Bremmer coupling series. *J. Math. Phys.*, 37:3246–3282, 1996.
- [4] J. T. Fokkema and P. M. van den Berg. *Seismic applications of acoustic reciprocity*. Elsevier, Amsterdam, 1993.
- [5] H. Jakubowicz. Wave equation prediction and removal of interbed multiples. In *Expanded Abstracts*, pages 1527–1530. Soc. Explor. Geophys., 1998.
- [6] B. A. Lippmann. Rearrangement collisions. *Phys. Rev.*, 102(1):264–268, 1956.
- [7] C. C. Stolk and M. V. de Hoop. Seismic inverse scattering in the downward continuation approach. *submitted to SIAM J. Appl. Math.*, 2005. CWP469P.
- [8] A. P. E. ten Kroode. Prediction of internal multiples. *Wave Motion*, 35:315–338, 2002.
- [9] D. J. Verschuur and A. Berkhout. Estimation of multiple scattering by iterative inversion, part II: Practical aspects and examples. *Geophysics*, 62(5):1596–1611, 1997.
- [10] A. Weglein, F. A. Gasparotto, P. M. Carvalho, and R. H. Stolt. An inverse-scattering series method for attenuating multiples in seismic reflection data. *Geophysics*, 62:1975–1989, 1997.

## Acknowledgments

We acknowledge the many useful discussions with Ken Larner and Kris Innanen. This work was supported by Total and the sponsors of the Consortium Project on Seismic Inverse Methods for Complex Structures at the Center for Wave Phenomena.